JOURNAL OF AGRICULTURAL AND FOOD CHEMISTRY
ARTICLE

J. Agric. Food Chem. 2010, 58, 11463–11470 11463
DOI:10.1021/jf102496p

Characterization of Graininess Formed in All Beef Tallow-Based Shortening

Zong Meng, Yuan-Fa Liu, Qing-Zhe Jin, Jian-Hua Huang, Zhi-Hua Song, Feng-Yan Wang, and Xing-Guo Wang*

State Key Laboratory of Food Science and Technology, School of Food Science and Technology, Jiangnan University, 1800 Lihu Road, Wuxi 214122, Jiangsu Province, People's Republic of China

A batch of all beef tallow (BT)-based model shortening (divided into six rectangular block samples) was stored under temperature fluctuation cycles of 5−20 °C until granular crystals were observed. The lipid composition, thermal properties, and polymorphism of the granular crystals and their surrounding materials were evaluated. Furthermore, the isothermal crystallization behavior of two parts noted above was also examined by pulsed nuclear magnetic resonance (pNMR), rheology, and polarized light microscopy (PLM). The changes of nanostructure including the aggregation of high-melting triacylglycerols (TAGs) and transformation into the most stable β polymorph occurred in granular crystals compared with surrounding materials. Concomitantly, a slower crystallization rate with a simultaneous increase in crystal growth led to the formation of large crystals and further aggregated to larger granular crystals when the size ultimately exceeded the sensory threshold.

KEYWORDS: Graininess; beef tallow; triacylglycerols; polymorphism; crystallization behavior

INTRODUCTION

In bakery shortening and margarine manufacturing, beef tallow (BT) is commonly used as one of the ingredients of the fat phase due to its advantageous properties, such as ideal lasting plasticity, typical aroma after baking, and high thermal and oxidative stability. However, the use of BT for solid fats in plastic fat products has encountered serious structural defects, particularly the growth of granular crystals in shortenings and margarines, which impair the consistency and plasticity of fat products. These granular crystals with diameters of 0.1−3 mm or even bigger are easily formed during handling, storage, and transportation of BT-based shortenings and margarines. This phenomenon is also termed graininess formation, which can be detected by consumers by rubbing the product between the fingers or when the product melts in the mouth. Thus, control of granular crystal formation in high-fat formulations is a very important point in the plastic fats industry.

The formation of granular crystals in palm oil-based fat blends has been investigated extensively (*1*−*4*). Ishikawa et al. (*1*) studied the formation of granular crystals in relation to palm oil and concluded that palm oil transformation into the β polymorph might be the reason for the formation of granular crystals in margarines. Watanabe et al. (*2*) reproduced the formation of granular crystals using a model fat blend consisting of 1,3-dipalmitoyl-2-oleoylglycerol (POP) and rapeseed oil. They showed that the POP content in granular crystals was higher than that in their surrounding materials and observed that the most stable β_1 polymorph of POP contributes to the formation of granular crystals. Miura et al. (*3*) studied the composition of granular crystals in margarine produced with an excess of palm oil, showing that POP was one of the major triacylglycerols (TAGs) present in the granular crystals. Tanaka et al. (*4*) investigated the crystallization behavior of palm oil and tripalmitin (PPP) in a model margarine system. The results suggest that the agglomeration of high melting point TAGs led to the formation of granular crystals in margarines. Only Jin et al. (*5*) studied the granular crystals in BT-based shortening, suggesting that the agglomerates of high melting point TAGs in the shortening formed with fluctuation of temperature cause the formation of β form granular crystals. The above-cited studies showed graininess formation in plastic fats closely related to the aggregations of high melting point TAGs with simultaneous transformation to the more stable β crystal polymorph. However, a fundamental question of how the graininess on the micrometer scale is connected with the TAGs and polymorph on the molecular scale is still unclear. The exact mechanism of the formation of granular crystals in the shortening and margarine is still to be illuminated. To fully understand the crystallization behavior of BT and its role in the formation of granular crystals in BT-based plastic fats, the structure hierarchy in granular crystals, which are structured by an underlying fat crystal network, must be clarified.

According to the studies of Tang and Marangoni (*6*, *7*), the fat crystal network is formed by the aggregation of fat crystals through van der Waals attraction. This aggregation process proceeds until a continuous three-dimensional network is formed, which is ultimately responsible for the macroscopic properties of the fat system, such as hardness, whippability, spreadability, graininess formation, brittleness, and aeration properties. The lipid composition (the fatty acid and TAG composition), directly under the influence of the mechanical treatment and temperature history, the polymorphic behavior of the fat crystals, the size and shape

*Corresponding author [telephone (086)510-85876799; fax (086)510-85876799; e-mail wxg1002@hotmail.com].

Published on Web 10/07/2010

of the crystals, and the nature of the crystal network will affect the macroscopic properties of plastic fats, just as the structure hierarchy of fat crystal networks brought forward by Tang and Marangoni (*6*).

Within this framework, in the present study granular crystals were reproduced in an all BT-based model shortening. Following the structure hierarchy of fat crystal networks, the lipid composition, thermal properties, polymorphism, crystallization behavior, crystal morphology, and crystal network of granular crystals and their surrounding materials were investigated systematically. Therefore, the present study may be able to give a better understanding of the mechanism causing the graininess phenomenon in BT-based plastic fat products.

MATERIALS AND METHODS

Materials. A batch of commercial all BT-based shortening was generously provided by Kerry Specialty Fats Ltd. (Shanghai, China) as the model shortening. Raw BT (Australian Tallow Exporting Ltd., Melbourne) was imported from Australia. Supelco 37 Component FAME Mixture was purchased from Sigma-Aldrich China (Shanghai, China). All other reagents and solvents were of analytical or chromatographic grade purchased from Sinopharm Chemical Reagent Co. Ltd. (Shanghai, China) to suit analytical requirements.

Induction of Granular Crystals in Model Shortenings. A whole batch of shortening was divided into six rectangular block samples (10 cm × 10 cm × 8 cm) as the model shortenings. Then, three of the model shortenings were stored in a KBF115 programmable oven (Binder, Tuttlingen, Germany) at a temperature fluctuation cycle of 5 °C for 12 h and 20 °C for another 12 h, until granular crystals were observed visually. These induction procedures were performed in duplicate (*2*, *3*). About 15 g of granular crystals (∼2−3 mm) was picked from the inside of each shortening by tweezers and placed into the sample cell. All operations were performed at 20 °C, in a temperature-controlled room to reduce the risk of melting the granular crystals. A portion (∼3−4 g) of granular crystals was subjected to both fatty acid and TAG compositions analyses; the other portion (∼11−12 g) was maintained in its original state at 5 °C for 24 h and then characterized by differential scanning calorimetry (DSC), X-ray diffraction (XRD), pulsed nuclear magnetic resonance (pNMR), oscillatory rheology, and polarized light microscopy (PLM) analyses. The materials (∼15 g) surrounding the granular crystals were also analyzed in terms of all the above-mentioned indices.

Fatty Acid Composition. Fatty acid methyl esters (FAMEs) were prepared according to AOCS Official Method Ce 2-66 (*8*) and subsequently analyzed with a GC-14B gas chromatograph (GC) equipped with a flame ionization detector (Shimadzu, Tokyo, Japan) and a fused-silica capillary column (CP-Sil88, 100 m × 0.25 mm × 0.2 mm). The temperatures of the injection port and detector were set at 250 °C. The column was heated to 120 °C and held for 3 min, then programmed at 8 °C/min to 175 °C, held for 28 min, increased to 215 °C at 3 °C/min, and held for 20 min. The fatty acid species were identified using the retention time of a FAME standard solution.

TAG Composition. TAGs were separated by reversed-phase high-performance liquid chromatography (HPLC). A Nova-Pak RP-C18 column (150 mm × 4.6 mm, particle size = 4 μm) (Waters, Milford, MA) with acetonitrile/dichloromethane (65:35, v/v) as the eluent at a flow rate of 1.0 mL/min and an evaporative light scattering detector (ELSD) was used. TAGs were identified by high-performance liquid chromatography−atmospheric pressure chemical ionization mass spectrometry (HPLC-APCI-MS). The HPLC conditions were the same as described before. A Platform ZMD 4000 (Waters) mass spectrometer (MS) equipped with an APCI interface was run at APCI source block and probe temperatures of, respectively, 100 and 400 °C and an MS multiplier voltage of 700 V. The measurement range was between m/z 250 and 1200. Quantitative determination of individual TAGs in fat blends was performed using HPLC following the procedures of Chen et al. (*9*).

DSC. The thermal properties of the samples were measured using a Mettler Toledo DSC 1 (Mettler Toledo, Schwerzenbach, Switzerland). Samples were hermetically sealed in an aluminum pan with an empty pan serving as reference. The samples were held at −40 °C for 5 min, and the melting profile was obtained by heating to 80 °C at 5 °C/min. After a 5 min hold at this temperature, the crystallization profiles were obtained by cooling to −40 °C at 5 °C/min.

Crystal Polymorphism by XRD. The polymorphic forms of fat crystals in the blends were determined by D8 Advance XRD (Bruker, Karlsrube, Germany), using Cu Kα radiation with Ni filter (k = 1.54056 Å; voltage, 40 kV; current, 40 mA; fixed 1.0, 1.0, and 0.1 mm divergence, antiscatter, and receiving slits, respectively). Samples were scanned from 1 to 30° (2θ scale) at a rate of 2.0°/min. The analyses were performed at ambient temperature.

pNMR. Solid fat content (SFC) was measured by pNMR using a Bruker PC120 series NMR analyzer (Bruker, Karlsruhe, Germany). The water bath based cooling used in the pNMR experiments also offered rapid cooling and accurate temperature control. The instrument was automatically calibrated using three standards (supplied by Bruker) containing 0, 31.3, and 74.6% solid. Samples were run in triplicate, and the values were averaged. The SFC of the samples was determined using the following thermal treatment: NMR tubes were filled with the melted fat sample (about 2.5 g), kept at 80 °C for 30 min, and then placed in a thermostated water bath at 5, 10, 15, 20, 25, 30, and 35 °C; SFC readings were obtained at appropriate time intervals.

The crystallization curves obtained under isothermal conditions were fitted to the Avrami equation. The Avrami equation can be used to quantify crystallization kinetics and give an indication of the nature of the crystallization process, including nucleation and growth. It has the form

$$-\ln(1-f) = Kt^n \quad (1)$$

where f is the fraction of crystal transformed at time t during crystallization, K is the crystallization rate constant, which depends primarily on crystallization temperature, and n is the Avrami exponent, a constant relating to the dimensionality of the transformation. The values of K and n are calculated from the intercept and slope, respectively, by the linear form of the Avrami equation as follows:

$$\ln[-\ln(1-f)] = n\ln t + \ln K \quad (2)$$

The numerical value of K is directly related to the half-time of crystallization, $t_{1/2}$, and therefore the overall rate of crystallization (*10*), which is given by the following equation:

$$(t_{1/2})^n = 0.693/K \quad (3)$$

Oscillatory Rheology. The rheological properties of the samples were determined using an AR1000 rheometer (TA Instruments, New Castle, DE) fixed with a water circulator at the base of a 2 cm parallel-plate geomety. Oscillation measurements were conducted at a constant frequency of 1 Hz and a constant stress of 6000 Pa (midpoint of the linear viscoelastic region (LVR)). The low frequency of 1 Hz was preferred to influence the crystallization as little as possible while maintaining enough data points (*11*). At the end of each experiment, an amplitude sweep was performed on the crystallized sample to check whether the requirement of LVR was still fulfilled. The melted sample was mounted on the temperature-controlled measuring plate, and the following temperature profile was applied: isothermal for 10 min at 70 °C to erase all crystal memory; cooling at 20 °C/min to the desired crystallization temperature; oscillatory time sweep at the achieved crystallization temperature (isothermal period). Rheograms were constructed by plotting the complex modulus ($|G^*|$) of the crystallizing sample as a function of isothermal time at the corresponding crystallization temperature (5, 10, 15, 20, 25, 30, and 35 °C).

Crystal Morphology by PLM. The morphology of crystallized samples was observed using PLM (DMRX, Leica, Germany) with a Canon A640 digital camera attached (Canon, Tokyo, Japan). The microstructures of samples of the granular crystals and their surrounding materials were imaged at 35 °C. The samples were held at 80 °C for 30 min to erase crystal memory. A small droplet (about 10 μL) of melted fat was placed on a clean glass slide preheated to the temperature of the molten fat, using a preheated glass capillary tube. A similarly heated glass coverslip was then placed on the surface of the droplet to produce a film of uniform thickness, avoiding the introduction of air bubbles into the sample. Samples were then cooled on a Linkam LTS-350 hot/cold stage (Linkam Instruments, Tadworth, U.K.) from 80 to 35 °C at 30 °C/min and

Table 1. Fatty Acid Composition (%) of Granular Crystals, Surrounding Materials, and Shortening[a]

fatty acid	granular crystals	surrounding materials	shortening
$C_{14:0}$	3.09 ± 0.03^{A}	2.50 ± 0.01^{B}	2.32 ± 0.01^{C}
$C_{16:0}$	40.18 ± 0.11^{A}	34.94 ± 0.09^{B}	34.42 ± 0.15^{C}
$C_{16:1}$	1.15 ± 0.02^{A}	0.96 ± 0.01^{B}	0.88 ± 0.01^{C}
$C_{17:0}$	0.79 ± 0.02^{A}	0.69 ± 0.03^{B}	0.71 ± 0.01^{B}
$C_{17:1}$	0.17 ± 0.01^{A}	0.20 ± 0.01^{B}	0.21 ± 0.01^{B}
$C_{18:0}$	16.20 ± 0.07^{A}	14.11 ± 0.05^{B}	14.79 ± 0.03^{C}
$C_{18:1}$*trans*	0.87 ± 0.03^{A}	1.56 ± 0.01^{B}	1.66 ± 0.02^{C}
$C_{18:1}$	27.19 ± 0.13^{A}	30.76 ± 0.09^{A}	30.91 ± 0.10^{A}
$C_{18:2}$*trans*	0.13 ± 0.01^{A}	0.16 ± 0.01^{B}	0.17 ± 0.01^{B}
$C_{18:2}$	5.76 ± 0.03^{A}	8.51 ± 0.03^{B}	8.39 ± 0.03^{C}
$C_{20:0}$	0.28 ± 0.03^{A}	0.25 ± 0.01^{A}	0.28 ± 0.01^{A}
$C_{20:1}$	0.15 ± 0.02^{A}	0.18 ± 0.01^{A}	0.20 ± 0.03^{A}
$C_{18:3}\omega 3$	0.34 ± 0.01^{A}	0.55 ± 0.01^{B}	0.54 ± 0.01^{B}
others[b]	3.70 ± 0.03^{A}	4.63 ± 0.02^{B}	4.52 ± 0.03^{C}
$\sum$ TFA[c]	1.00 ± 0.01^{A}	1.72 ± 0.02^{B}	1.83 ± 0.04^{C}
$\sum$ SFA[d]	60.54 ± 0.33^{A}	52.49 ± 0.24^{B}	52.52 ± 0.19^{B}
$\sum$ USFA[e]	34.76 ± 0.17^{A}	41.16 ± 0.16^{B}	41.13 ± 0.11^{B}

[a] Different superscript letters (A−C) denote significantly different groups ($P < 0.05$), whereas the same letters denote similar groups ($P > 0.05$) in the same row. [b] "Others" refers to other fatty acids not identified by the FAME standards. [c] Σ TFA: sum of trans fatty acids. [d] Σ SFA: sum of saturated fatty acids. [e] Σ USFA: sum of unsaturated fatty acids; Σ USFA was calculated except trans fatty acids in lipids.

observed under the microscope for up to 90 min. The photomicrograph of the crystal was taken at 400× magnification.

The images acquired were then inverted, thresholded, and analyzed using ImageJ 1.36b software that is available in the public domain of the National Institutes of Health (*12*). The fractal dimension was determined using a box counting algorithm, which was calculated as the negative of the slope of the linear regression curve of the log−log plot of the number of occupied boxes N_b versus the side length L_b, with the result denoted D_b.

Statistical Analysis. Triplicate analyses ($n = 6$ for granular crystals, surrounding materials, and shortening, respectively) were performed for each dependent variable (fatty acid composition, TAG composition, thermal property, crystal polymorphism, SFC, oscillatory rheology, and crystal morphology). Analysis of variance (ANOVA) with Duncan's multiple-range test was carried out by the Statistical Analysis System software (SAS, Cary, NC). Differences were considered to be significant at $P < 0.05$. Values shown in **Tables 1−3** are the means of triplicates ± standard deviations.

RESULTS AND DISCUSSION

Lipid Composition. The fatty acid compositions of the granular crystals, surrounding materials, and shortening are given in **Table 1**. The composition of the shortening was in agreement with the BT fatty acid ranges published in the literature (*13*), which can be explained by the fact that BT was the only base stock of the shortening product. As shown in **Table 1**, only small differences were detected between the surrounding materials and the whole shortening ($P < 0.05$). Compared to the surrounding materials, the granular crystals contained a significantly higher content of high melting point saturated fatty acids ($P < 0.05$), for example, myristic ($C_{14:0}$), $C_{16:0}$, margaric ($C_{17:0}$), $C_{18:0}$, and arachidic acid ($C_{20:0}$), and a significantly lower content of low melting point unsaturated fatty acids ($P < 0.05$), for example, oleic ($C_{18:1}$) and linoleic ($C_{18:2}$) acid. Thus, concomitantly, the granular crystals contained 60.54% the total saturated fatty acids (Σ SFA), higher than the surrounding materials of 52.49% ($P < 0.05$); meanwhile, the former contained 34.76% total unsaturated fatty acids (Σ USFA), lower than 41.16% ($P < 0.05$). It was likely that high melting point SFA, for example, $C_{16:0}$ and $C_{18:0}$, may be the key factors for the structural defects of the shortening, as reported by other researchers (*4*). Trans fatty acids were reported to decrease the level of structural order of the crystals and also impart a certain faster crystallization and smaller crystals to the fat (*14*, *15*). However, the small differences ($P < 0.05$) in the total trans fatty acids (Σ TFA) between the granular crystals and the surrounding materials are essentially negligible, which may not fully support the major crystal structure differences between them.

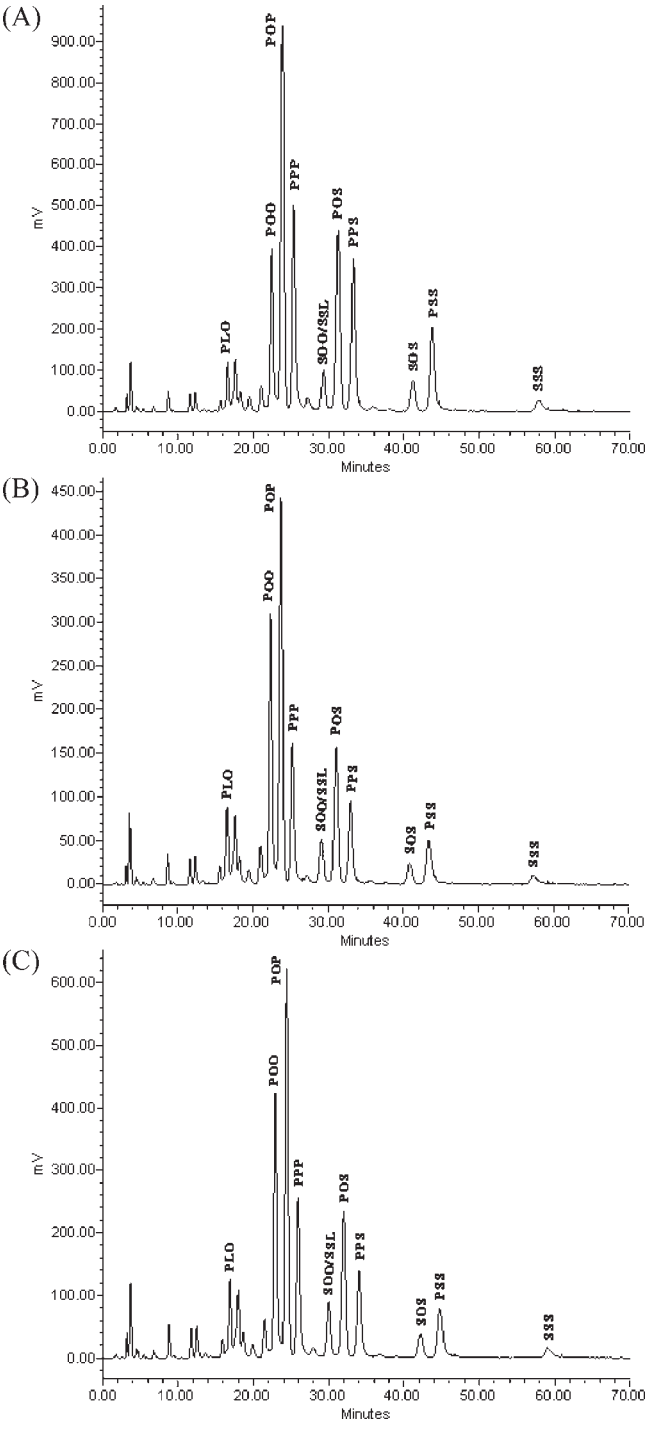

Figure 1. HPLC chromatograms of granular crystals (**A**), surrounding materials (**B**) and shortening (**C**). P, palmitoyl; L, linoleoyl; O, oleoyl; S, stearoyl.

Figure 1 shows the TAG profiles of the granular crystals, surrounding materials, and shortening obtained by HPLC. The change in TAG profiles among the three samples noted above was obvious; that is, the relative concentrations of several TAGs increased while others were observed to decrease ($P < 0.05$) by

Table 2. TAG Composition (%) of Granular Crystals, Surrounding Materials, and Shortening

TAG[a]	granular crystals	surrounding materials	shortening	$[M + Na]^{+b}$	$[DG]^{+b}$	$[DG]^{+b}$	$[DG]^{+b}$
PLO	2.44 ± 0.12	4.22 ± 0.17	4.17 ± 0.13	880	$[PL]^+$ 576	$[LO]^+$ 602	$[PO]^+$ 578
POO	10.34 ± 0.37	17.76 ± 0.28	17.19 ± 0.46	882	$[PO]^+$ 578	$[OO]^+$ 604	
POP	24.11 ± 0.33	26.59 ± 0.40	24.77 ± 0.34	856	$[PO]^+$ 578	$[PP]^+$ 552	
PPP	14.01 ± 0.21	10.36 ± 0.40	11.34 ± 0.29	830	$[PP]^+$ 552		
SOO/SSL	3.06 ± 0.10	3.58 ± 0.12	4.20 ± 0.17	910	$[SO]^+$ 606	$[OO]^+$ 604	
				910	$[SS]^+$ 608	$[SL]^+$ 604	
POS	14.48 ± 0.53	11.58 ± 0.31	11.78 ± 0.26	884	$[PO]^+$ 578	$[SO]^+$ 606	$[PS]^+$ 580
PPS	11.57 ± 0.28	6.92 ± 0.15	7.21 ± 0.24	858	$[PP]^+$ 552	$[PS]^+$ 580	
SOS	2.99 ± 0.17	2.22 ± 0.09	2.29 ± 0.25	912	$[SO]^+$ 606	$[SS]^+$ 608	
PSS	7.38 ± 0.24	4.66 ± 0.18	5.09 ± 0.27	886	$[PS]^+$ 580	$[SS]^+$ 608	
SSS	1.05 ± 0.06	0.92 ± 0.02	0.97 ± 0.08	914	$[SS]^+$ 608		

[a] Proposed TAG structure (see **Figure 1** for abbreviations). [b] Sodium adduct molecular ion and fragment ions as detected by APCI-MS.

comparison of the granular crystals (**Figure 1A**) with the surrounding materials (**Figure 1B**) and shortening (**Figure 1C**). The results obtained were similar to previous findings by Jin et al. (*5*). This change indicated that the migration and aggregation of some TAGs had occurred in the shortening and thus led to the different TAG composition between granular crystals and surrounding materials.

Proposed TAG structures giving rise to the peaks shown (**Figure 1**) are listed with the corresponding mass identification data in **Table 2**. Designation of structure for TAGs under each chromatographic peak was made from reversed-phase HPLC-APCI-MS analysis of the observed TAG corresponding sodium adducts of the molecular ions $[M + Na]^+$ and one fatty acyl moiety cleaved ions $[M - (R - COO)]^+$ ($[DG]^+$). The mass spectra for individual TAGs are not shown to conserve space.

Four trisaturated (S_3) TAGs in the shortening, that is, PPP, PPS, PSS, and SSS, at 11.34, 7.21, 5.09, and 0.97%, respectively, were reduced to 10.36, 6.92, 4.66, and 0.92% in surrounding materials, but increased to 14.01, 11.57, 7.38, and 1.05% in the granular crystals. Simultaneously, several disaturated−monounsaturated (S_2U) TAGs, such as POS and SOS, were observed to undergo similar changes. The contents of POS and SOS in the shortening were 11.78 and 2.29%, respectively, which were reduced to 11.58 and 2.22% in the surrounding materials and increased to 14.48 and 2.99% in the granular crystals, respectively. Concomitantly, opposite changes were observed in the proportion of several other lower melting S_2U and monosaturated−diunsaturated (SU_2) TAGs, such as POP, SOO/SSL, PLO, and POO, which were reduced from 24.77, 4.20, 4.17, and 17.19% in the shortening to 24.11, 3.06, 2.44, and 10.34% in the granular crystals, respectively.

The results indicated that the higher melting TAGs, such as S_3 PPP, PPS, PSS, and SSS and S_2U POS and SOS, had gathered together to form the granular crystals as the driving force provided by the temperature fluctuation. Lower melting TAGs will melt when the storage temperature is high, whereas the higher melting TAGs are still in their crystal state. This may have enabled the crystals of these molecules to migrate and agglomerate to form larger crystals. Meanwhile, lower melting TAGs will be excluded into the surrounding materials, as observed by the TAG composition analysis.

Melting and Crystallization Properties. Both fatty acid and TAG composition contribute to the melting and crystallization properties of the fat blends. The changes in the TAG composition of the granular crystals and surrounding materials have concomitant effects on their melting properties. A broad endothermic peak and three sharp endothermic peaks were observed in the granular crystals (curves not shown to conserve space), corresponding to peak temperatures (T_p) of −5.54, 12.43, 22.02, and 42.09 °C, respectively. The required enthalpy variation (ΔH, J/g) in each big peak of the granular crystals was 4.56, 22.06, 5.64, and 30.31 J/g. The melting thermograms of the surrounding materials show that a broad endothermic peak and two sharp endothermic peaks at −4.44, 11.88, and 41.62 °C corresponding ΔH were 7.50, 10.00, and 28.17 J/g, respectively, and the sharp peak near 22.00 °C disappeared. The two parts had very similar crystallization profile shapes, and all displayed a sharp exothermic peak (T_p = 26.5 °C and ΔH = 12.79 J/g for granular crystal parts; T_p = 25.10 °C and ΔH = 11.68 J/g for surrounding material parts) and a broad exothermic peak (T_p = 5.41 °C and ΔH = 10.77 J/g for granular crystal parts; T_p = 4.97 °C and ΔH = 19.57 J/g for surrounding material parts). Therefore, the granular crystal parts crystallized and melted at higher temperature zone with an increased ΔH and at lower temperature zone with a decreased ΔH compared with the surrounding material parts ($P < 0.05$) because it contained more higher melting and less lower melting TAGs. In addition, changes in the shape of the melting profile could be indicative of changes in polymorphism. This suggested that the migration and aggregation of TAGs led to changes in polymorphic form. To confirm this, powder XRD was performed on the granular crystals and surrounding materials.

Crystal Polymorphism. XRD was used to identify crystal polymorphs by determining the long and short spacings of crystals. The short spacing of the α form appears near 4.15 Å, that of the β' form at 4.2 and 3.8 Å, and that of the β form at 4.6 Å (single strong spacing). Levels of β' and β crystals in mixtures were estimated by the relative intensity of the short spacings at 3.8, 4.2, and 4.6 Å (*16*). The long spacings of the fat samples indicated the lamellar packing structure of the fats (*17*).

The polymorphic forms of the granular crystals and surrounding materials were determined with the short (**Figure 2A**) and long spacings (**Figure 2B**). The surrounding materials had a mixture of both α and β' polymorphic forms, showing medium-strong intensities at 4.15 Å (for the α form) and 3.80 and 4.28 Å (for the β' form) when stored at 5 °C. The granular crystals displayed a relatively stronger short spacing peak at 4.56 Å, indicating the occurrence of β polymorph, together with medium-strong intensity peaks at 4.15 Å (for the α form) and 3.80 and 4.28 Å (for the β' form), which indicated that polymorph transition from metastable β' to stable β has occurred in the granular crystals. There was a long spacing peak observed in both granular crystals and surrounding materials at 36.48 and 37.09 Å, respectively. Both samples showed packing near 37.00 Å with a third-order reflection at 13.67 Å. Meanwhile, two relatively weaker signals existed only in the granular crystals at 49.13 and 28.27 Å. This indicated that the longitudinal packing state of TAGs in the granular crystals had undergone changes to a certain degree as compared with the surrounding materials. This further showed that the size of the molecules in the TAGs and the angle of inclination between the axis of the TAG chain and its basal plane had been changed.

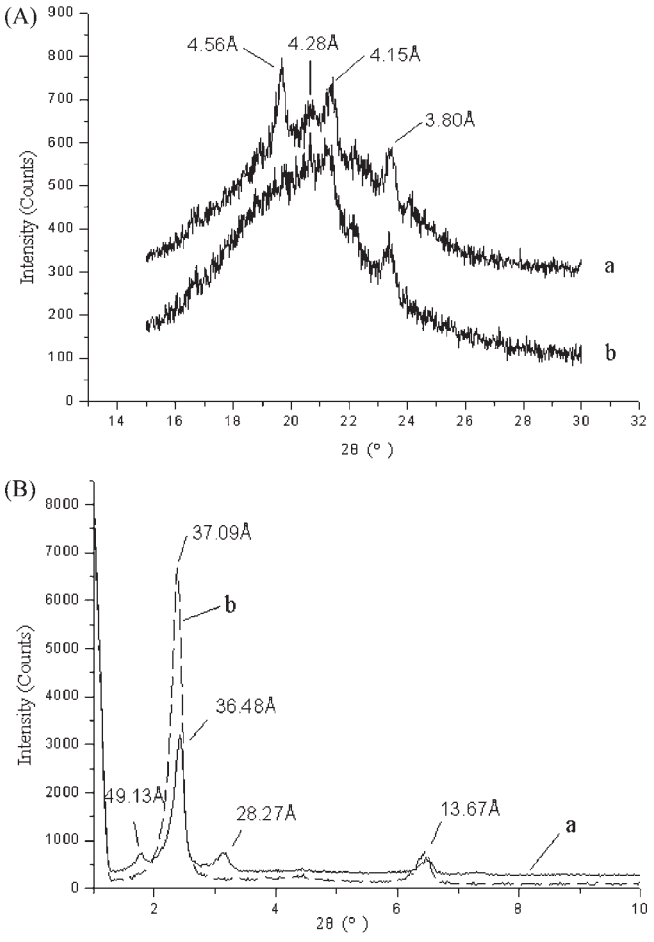

Figure 2. XRD spectra for short (**A**) and long spacings (**B**) of granular crystals (a) and surrounding materials (b).

To summarize, parts of the crystal converted to more stable β polymorphs and changes of TAG packing had occurred in the granular crystals, which were associated with an increase in the content of S_3 TAGs such as SSS and PPP and S_2U TAGs such as POS and SOS (mainly β-tending crystals) and a significant decrease in the content of SU_2 TAGs such as PLO and POO (mainly β'-tending crystals) (*18*). The results suggested that agglomeration of the high melting point crystals occurred, and concomitantly the transformation into the most stable β polymorph took place with the temperature fluctuations. All of the changes combined could lead to the formation of granular crystals. However, the exact mechanisms on how the granular crystals on the micrometer scale connected with the TAGs and polymorph on the nanostructure scale were still unclear and needed to be illuminated.

Crystallization Kinetics. The isothermal crystallization behavior of the surrounding materials and granular crystals was investigated with several techniques, namely, pNMR, oscillatory rheology, and PLM.

Figure 3 presents the SFC as a function of time for the surrounding materials (**Figure 3A**) and the granular crystals (**Figure 3B**). Both parts crystallized very rapidly at high supercooling (crystallization temperature below 25 °C), showing hyperbolic patterns against time, and an equilibrium value in SFC was clearly visible in all curves. However, when the temperature was brought above 25 °C, there appeared an induction time when no fat crystallized, followed by a period of more rapid crystallization, and sigmoidal curves were found. In addition, comparison of the curves of the surrounding materials and granular

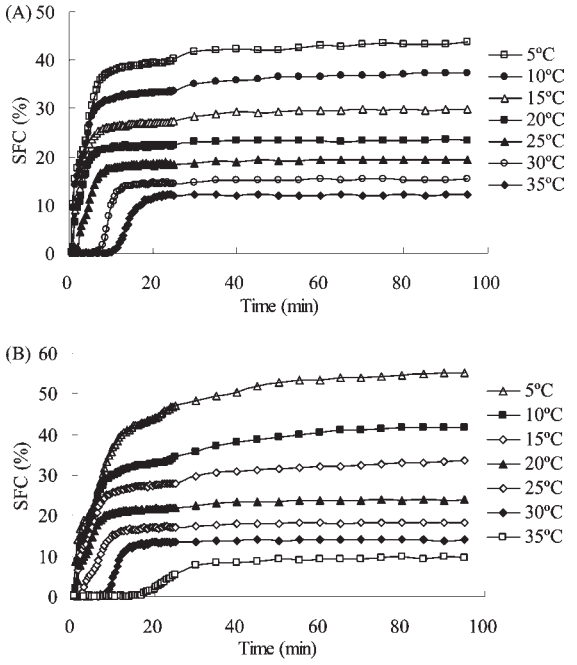

Figure 3. SFC versus time profile during isothermal crystallization of surrounding materials (**A**) and granular crystals (**B**) at different crystallization temperatures.

crystals clearly showed that the former has a steeper slope at each corresponding temperature, which indicated that the surrounding materials have faster crystallization rates and shorter times to achieve maximum SFC. This distinction was most obvious at 35 °C, after isothermal crystallization of 20 min; the crystal of the surrounding materials was almost stable, whereas the granular crystal parts just generated the nuclei and began the crystal growth at the mentioned time.

Differences in the crystallization kinetics of the surrounding materials and granular crystals under isothermal conditions are shown in **Table 3**. As can be observed, the SFC data fit the equation very well over the entire crystallization range ($R^2 > 0.99$ in all cases). As expected, K decreased with increasing crystallization temperature. When surrounding materials were at 30 and 35 °C, crystallization temperature had a very strong influence on K ($P < 0.001$); the Avrami constant dropped by factors of roughly 10^2 and 10^3 compared to the value at 25 °C, respectively. The crystallization temperature had also shown a very strong impact on K in granular crystals at 30 and 35 °C ($P < 0.001$); the Avrami constant dropped by factors of roughly 10^3 and 10^5 compared to the value at 25 °C, respectively. The decreasing K values also indicate a change in the nucleation and/or growth rate in the two parts in the range of 25−35 °C because K values are a combined function of nucleation and growth as well as a strong function of temperature, which inevitably induces changes in crystal morphology, such as crystal size and type. The increase in $t_{1/2}$ for the two parts as a function of increasing crystallization temperature also reflects the decrease in K at higher temperatures. By comparing the K and $t_{1/2}$ of the surrounding materials and granular crystals in each crystallization temperature, it can be found that the former has higher K values and lower $t_{1/2}$ values ($P < 0.05$). This indicated that granular crystals showed a slower crystallization rate at all isothermal crystallization temperatures, which was in agreement with previous isothermal crystallization curves (**Figure 3**).

As shown in **Table 3**, the Avrami exponent n for both the surrounding materials and granular crystals increased with increasing

Table 3. Avrami Exponents (n), Avrami Constants (K), and Half-Times of Crystallization ($t_{1/2}$) for Surrounding Materials and Granular Crystals at Different Crystallization Temperatures

temperature (°C)	n	K (min^{-n})	$t_{1/2}$ (min)	R^2
		Surrounding Materials		
5	0.795 ± 0.024	0.316 ± 0.011	2.687 ± 0.185	0.999
10	0.911 ± 0.021	0.279 ± 0.009	2.713 ± 0.163	0.994
15	1.123 ± 0.047	0.222 ± 0.011	2.754 ± 0.056	0.993
20	1.278 ± 0.035	0.188 ± 0.005	2.778 ± 0.148	0.998
25	1.868 ± 0.064	0.045 ± 0.004	4.335 ± 0.203	0.996
30	3.220 ± 0.121	$6.14 \times 10^{-4} \pm 2.71 \times 10^{-5}$	8.872 ± 0.414	0.999
35	3.479 ± 0.145	$8.62 \times 10^{-5} \pm 3.11 \times 10^{-6}$	13.264 ± 0.634	0.995
		Granular Crystals		
5	1.094 ± 0.012	0.203 ± 0.006	3.066 ± 0.125	0.997
10	1.254 ± 0.041	0.167 ± 0.005	3.108 ± 0.056	0.999
15	1.342 ± 0.051	0.136 ± 0.007	3.373 ± 0.211	0.998
20	1.737 ± 0.073	0.057 ± 0.002	4.196 ± 0.086	0.996
25	2.023 ± 0.054	0.016 ± 0.001	6.402 ± 0.316	0.994
30	4.334 ± 0.079	$2.36 \times 10^{-5} \pm 1.11 \times 10^{-6}$	10.741 ± 0.524	0.997
35	4.461 ± 0.122	$4.46 \times 10^{-7} \pm 1.81 \times 10^{-8}$	24.431 ± 0.538	0.993

crystallization temperature, whereas at a set temperature, the value of n was slightly higher in the granular crystals ($P < 0.05$). This parameter reflects the details of fat crystal nucleation and growth mechanisms. Cheong et al. (*19*) tabulated values for n for various types of nucleation and growth. Nucleation can be instantaneous, with the nuclei appearing all together at the beginning of the process, or sporadic, with the number of nuclei increasing linearly with time. Growth occurs in the form of rods, disks, or spherulites in one, two, or three dimensions, respectively (*20*). For the surrounding materials and granular crystals individually, an increase in n from ~1 to ~4 with increasing temperature can also be due to the type of fat crystal growth from rod-like at higher degrees of supercooling to spherulitic form at lower degrees of supercooling. Meanwhile, the sharp change in n around 30 °C in the surrounding materials and granular crystals suggests the existence of different crystallization mechanisms depending on the degree of supercooling. The change in n at this point also indicated differences in crystal growth geometry and possibly the type of nucleation.

Oscillatory Rheology. The isothermal crystallization mechanism was further investigated with oscillatory rheology experiments. This method allows recording all three steps of the crystallization process, namely, primary crystallization, microstructural development of the fat crystal network, and macroscopic properties (*11*). Crystallization curves were obtained by plotting the complex modulus ($|G^*|$) as a function of isothermal time at the corresponding crystallization temperature (5, 10, 15, 20, 25, 30, and 35 °C), which is illustrated in **Figure 4**. The $|G^*|$, incorporating both the storage modulus (G') and the loss modulus (G''), can be used to evaluate the overall structure of the system. $|G^*|$ can be defined as the ratio of the shear stress to the applied deformation and consists of real and imaginary components, respectively, G' and G''. G' is denoted the storage modulus and is indicative of the solid-like or elastic nature of a substance, whereas the loss modulus G'' is indicative of the liquid-like or viscous nature of a substance.

As shown in **Figure 4**, the changes in $|G^*|$ correspond with the time scale of the evolution of the SFC illustrated in **Figure 3**. Similar to crystallization curves by SFC, the surrounding materials and granular crystals showed hyperbolic curves for crystallization temperatures below 25 °C. Crystallization initially was fast. At temperatures above 25 °C, one step was observed in $|G^*|$ versus time curves for the two parts. As discussed by Toro-Vazquez et al. (*21*, *22*) and De Graef et al. (*23*), these different

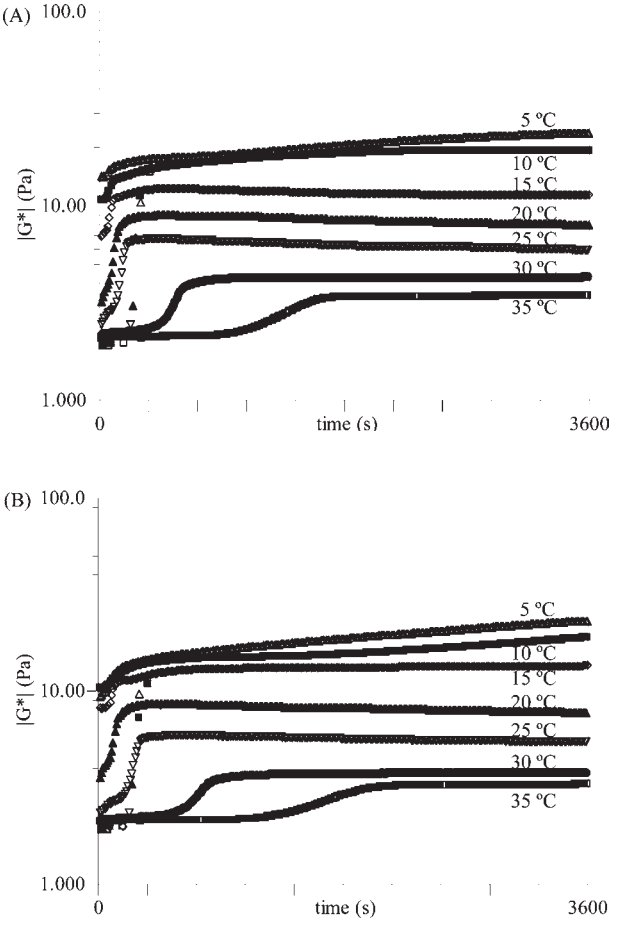

Figure 4. Complex modulus of surrounding materials (**A**) and granular crystals (**B**) as a function of isothermal time at different crystallization temperatures obtained with oscillatory rheology.

stages can be attributed to crystallization into different polymorphic forms. At first, low constant $|G^*|$ values illustrate the liquid state of the samples, then the fats gain structure as α crystals are formed; the $|G^*|$ maintains a trend to increase due to the polymorphic transition of α to β' crystals and the subsequent formation of β' crystals from the melt. Then the $|G^*|$ reaches an equilibrium value, which can be used to evaluate the macroscopic

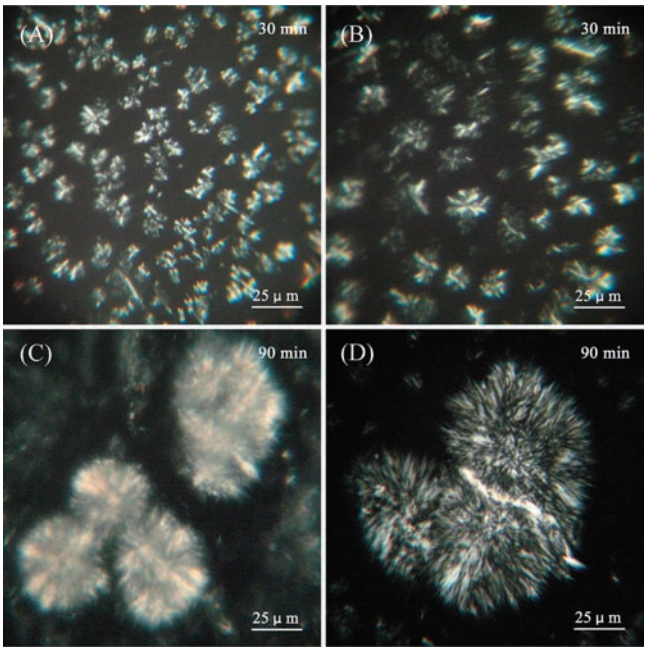

Figure 5. Polarized light micrographs of surrounding materials (**A**, **C**) and granular crystals (**B**, **D**) crystallized isothermally at 35 °C for 30 and 90 min.

properties of the sample; also, part of the crystal change into β crystals may have occurred. The increase in $|G^*|$ is due not only to the primary crystallization but also to the development of the microstructure by aggregation. These two processes occur simultaneously and cannot be separated completely. Especially, the ongoing crystallization and recrystallization cause a growing together of the flocculated crystals, thereby greatly strengthening the network, which can be seen as an increase in the $|G^*|$. When the rheological data of the two samples at various temperatures are compared, the main difference can be found in the time scale of events. On the basis of pNMR results, it was already clear that the surrounding materials crystallized more quickly than the granular crystals. This observation is also confirmed by the rheological data.

Kinetic Microscopy and Image Quantitative Analysis. The surrounding materials and granular crystals showed greater differences in crystallization kinetics at 35 °C. For a better explanation of the relationship between crystallization kinetics and mechanical properties of two samples, real-time PLM of the isothermal crystallization process at 35 °C was carried out.

Micrographs obtained after crystallization at 35 °C for 30 min for surrounding materials (**Figure 5A**) and granular crystals (**Figure 5B**) generated more significant differences in the number of crystals and the mean crystallite diameter. The granular crystal parts showed larger and less numerous spherical crystals relative to the surrounding materials. These microstructure results for the granular crystal were consistent with the trends observed in Avrami parameters (lower K and higher n) and longer induction times of nucleation. After isothermal crystallization for 90 min, large spherulitic microstructures (well-organized with needle-shaped crystals oriented radially from the center) of ~100 μm in diameter were present in the granular crystal parts. Similarly, a combination of small spherulites (~50 μm in diameter) and small needle-shaped crystals was observed in the surrounding materials. It was also found that the crystals aggregated and then continued to grow larger through further crystallization in granular crystal parts, leading to the formation of intermediately sized clusters, which further aggregate to form large clusters. This aggregation process is most probably controlled by mass and heat transfer limitations. In general, a decreased nucleation in the granular crystal parts is accompanied by an increase in crystal growth. The number, size, and shape of the particles and large clusters will define the microstructure, which will in turn determine the macroscopic properties of the fat, such as the structural defect—formation of large granular crystals.

Two-dimensional polarized light images of the samples depicted crystal clusters or single spherulites, but we were also interested in the spatial distribution of mass within the network. The fractal dimension (D_b) might be useful as a quantitative parameter, which may indicate overall complexity or scale dependency of pattern in the crystal network. Normally, higher fractal dimensions occur in networks that are more ordered, whereas networks that arise from a more disordered nucleation and growth process result in lower fractal dimensions (*24*). When crystallized isothermally at 35 °C for 30 and 90 min, D_b values were 1.893 and 1.938 for surrounding materials and 1.843 and 1.898 for granular crystals, respectively. The granular crystal parts showed lower D_b values than the surrounding materials during the isothermal crystallization ($P < 0.05$), suggesting that slow crystallization has changed the spatial distribution of crystals to a more disordered crystal network. D_b is also sensitive to the degree of fill within the network; therefore, higher D_b values indicate an increase in space-filling mass (i.e., the smaller, more numerous particles of the surrounding material parts fill more space relative to the larger, less numerous particles of the granular crystal parts during the isothermal crystallization). This indicated that the granular crystal parts assume sparse crystal space-filling, which was consistent with the polarized light images shown in **Figure 5**. PLM and image analysis displayed that during primary crystallization small crystals were formed which subsequently aggregated to a network structure. The strong increase in SFC and $|G^*|$ coincided with this network formation.

This study has shown that the migration and aggregation of higher melting TAGs, such as S_3 PPP, PPS, PSS, and SSS, S_2U POS and SOS, and, consequently, the changes of TAG packing and transformation into the most stable β polymorph took place as the driving force provided by the temperature fluctuation. These changes of nanostructure inducing the sample crystallization rate decreased and were accompanied by an increase in crystal growth. The crystals of high melting TAGs, which were still in their crystal state, aggregate and then continue to grow larger through further crystallization, leading to the formation of large clusters. The microstructure size of these crystal aggregates exceeded the sensory threshold, and the aggregates could be detected upon visual and physical examination (by rubbing between the fingers or melting in the mouth) and therefore impaired the sensory and functional properties of the finished products.

ABBREVIATIONS USED

BT, beef tallow; pNMR, pulsed nuclear magnetic resonance; PLM, polarized light microscopy; TAGs, triacylglycerols; POP, 1,3-dipalmitoyl-2-oleoylglycerol; PPP, tripalmitin; DSC, differential scanning calorimetry; XRD, X-ray diffraction; FAMEs, fatty acid methyl esters; GC, gas chromatography; HPLC, high-performance liquid chromatography; ELSD, evaporative light scattering detector; HPLC-APCI-MS, high-performance liquid chromatography−atmospheric pressure chemical ionization mass spectrometry; SFC, solid fat content; LVR, linear viscoelastic region; ANOVA, analysis of variance; Σ SFA, the total saturated fatty acids; Σ USFA, the total unsaturated fatty acids; Σ TFA, the total trans fatty acids; S_3, trisaturated; S_2U, disaturated−monounsaturated; SU_2, monosaturated−diunsaturated; T_p, peak temperature; ΔH, enthalpy variation; D_b, fractal dimension.

ACKNOWLEDGMENT

We gratefully acknowledge the technical assistance of Tao Guanjun of the State Key Laboratory of Food Science and Technology, Jiangnan University, during the HPLC-APCI-MS analysis. We thank Kerry Specialty Fats (Shanghai) Ltd. for providing materials for the experiments.

LITERATURE CITED

(1) Ishikawa, H.; Mizuguchi, T.; Kondo, S. Studies on granular crystals growing in palm oil. *J. Jpn. Oil Chem. Soc.* **1980**, *29*, 235−242.

(2) Watanabe, A.; Tashima, I.; Matsuzaki, N.; Kurashige, J.; Sato, K. On the formation of granular crystals in fat blends containing palm oil. *J. Am. Oil Chem. Soc.* **1992**, *69*, 1077−1080.

(3) Miura, S.; Konishi, H. Crystallization behavior of 1,3-dipalmitoyl-2-oleoyl-glycerol and 1-palmitoyl-2,3-dioleoyl-glycerol. *Eur. J. Lipid Sci. Technol.* **2001**, *103*, 804−809.

(4) Tanaka, L.; Miura, S.; Yoshioka, T. Formation of granular crystals in margarine with excess amount of palm oil. *J. Am. Oil Chem. Soc.* **2007**, *84*, 421−426.

(5) Jin, Q. Z.; Gao, H. Y.; Shan, L.; Liu, Y. F.; Wang, X. G. Study on grainy crystals in edible beef tallow shortening. *Food Res. Int.* **2007**, *40*, 909−914.

(6) Tang, D.; Marangoni, A. G. Microstructure and fractal analysis of fat crystal networks. *J. Am. Oil Chem. Soc.* **2006**, *83*, 377−388.

(7) Tang, D.; Marangoni, A. G. Computer simulation of fractal dimensions of fat crystal networks. *J. Am. Oil Chem. Soc.* **2006**, *83*, 309−314.

(8) AOCS. *Official Methods and Recommended Practices of the American Oil Chemists' Society*, 5th ed.; American Oil Chemists' Society: Champaign, IL, 1998; Ce 2-66.

(9) Chen, C. W.; Chong, C. L.; Ghazali, H. M.; Lai, O. M. Interpretation of triacylglycerol profiles of palm oil, palm kernel oil and their binary blends. *Food Chem.* **2007**, *100*, 178−191.

(10) Singh, A. P.; Bertoli, C.; Rousset, P. R.; Marangoni, A. G. Matching Avrami indices achieves similar hardnesses in palm oil-based fats. *J. Agric. Food Chem.* **2004**, *52*, 1551−1557.

(11) De Graef, V.; Foubert, I.; Smith, K. W.; Cain, F. W.; Dewettinck, K. Crystallization behavior and texture of trans-containing and trans-free palm oil based confectionery fats. *J. Agric. Food Chem.* **2007**, *55*, 10258−10265.

(12) National Institutes of Health, ImageJ 1.36b; http://rsb.info.nih.gov/ij.

(13) Raw materials. In *Fats and Oils—Formulating and Processing for Applications*, 3rd ed.; O'Brien, R. D., Ed.; CRC Press: Boca Raton, FL, 2009; pp 1−72.

(14) Vereecken, J.; Foubert, I.; Smith, K. W.; Dewettinck, K. Relationship between crystallization behavior, microstructure, and macroscopic properties in trans-containing and trans-free filling fats and fillings. *J. Agric. Food Chem.* **2007**, *55*, 7793−7801.

(15) Reyes-Hernández, J.; Dibildox-Alvarado, E.; Charó-Alonso, M.; Toro-Vazquez, J. Physicochemical and rheological properties of crystallized blends containing trans-free and partially hydrogenated soybean oil. *J. Am. Oil Chem. Soc.* **2007**, *84*, 1081−1093.

(16) Lee, J. H.; Akoh, C. C.; Himmelsbach, D. S.; Lee, K.-T. Preparation of interesterified plastic fats from fats and oils free of trans fatty acid. *J. Agric. Food Chem.* **2008**, *56*, 4039−4046.

(17) Campbell, S. D.; Goff, H. D.; Rousseau, D. Comparison of crystallization properties of a palm stearin/canola oil blend and lard in bulk and emulsified form. *Food Res. Int.* **2002**, *35*, 935−944.

(18) Lawler, P. J.; Dimick, P. S. Crystallization and polymorphism of fats. In *Food Lipids—Chemistry, Nutrition, and Biotechnology*, 3rd ed.; Akoh, C. C., Min, D. B., Eds.; CRC Press: New York, 2008; pp 245−266.

(19) Cheong, L.-Z.; Zhang, H.; Xu, Y.; Xu, X. Physical characterization of lard partial acylglycerols and their effects on melting and crystallization properties of blends with rapeseed oil. *J. Agric. Food Chem.* **2009**, *57*, 5020−5027.

(20) Wright, A.; Hartel, R.; Narine, S.; Marangoni, A. The effect of minor components on milk fat crystallization. *J. Am. Oil Chem. Soc.* **2000**, *77*, 463−475.

(21) Toro-Vazquez, J.; Herrera-Coronado, V.; Dibildox-Alvarado, E.; Charo-Alonso, M.; Gomez-Aldapa, C. Induction time of crystallization in vegetable oils, comparative measurements by differential scanning calorimetry and diffusive light scattering. *J. Food Sci.* **2002**, *67*, 1057−1064.

(22) Toro-Vazquez, J.; Pérez-Martínez, D.; Dibildox-Alvarado, E.; Charó-Alonso, M.; Reyes-Hernández, J. Rheometry and polymorphism of cocoa butter during crystallization under static and stirring conditions. *J. Am. Oil Chem. Soc.* **2004**, *81*, 195−202.

(23) Veerle De, G.; Koen, D.; Dirk, V.; Imogen, F. Rheological behavior of crystallizing palm oil. *Eur. J. Lipid Sci. Technol.* **2006**, *108*, 864−870.

(24) Lee, J.; Akoh, C.; Lee, K.-T. Physical properties of trans-free bakery shortening produced by lipase-catalyzed interesterification. *J. Am. Oil Chem. Soc.* **2008**, *85*, 1−11.

Received for review June 29, 2010. Revised manuscript received September 25, 2010. Accepted September 25, 2010. This work was supported by the National High Technology Research and Development Program (863 Program) of China (Contract 2010AA101506).